Linköping University Post Print

Layer Formation by Resputtering in Ti-Si-C Hard Coatings during Large Scale Cathodic Arc Deposition

Anders Eriksson, Jianqiang Zhu, Naureen Ghafoor, Mats Johansson, Jacob Sjölen,
Jens Jensen, Magnus Odén, Lars Hultman and Johanna Rosén

N.B.: When citing this work, cite the original article.

Original Publication:

Anders Eriksson, Jianqiang Zhu, Naureen Ghafoor, Mats Johansson, Jacob Sjölen, Jens Jensen, Magnus Odén, Lars Hultman and Johanna Rosén, Layer Formation by Resputtering in Ti-Si-C Hard Coatings during Large Scale Cathodic Arc Deposition, 2011, Surface & Coatings Technology, (205), 15, 3923-3930.
http://dx.doi.org/10.1016/j.surfcoat.2011.02.007
Copyright: Elsevier Science B.V., Amsterdam.
http://www.elsevier.com/

Postprint available at: Linköping University Electronic Press
http://urn.kb.se/resolve?urn=urn:nbn:se:liu:diva-61991

Layer Formation by Resputtering in Ti-Si-C Hard Coatings during Large Scale Cathodic Arc Deposition

A.O. Eriksson,[*,a] J.Q. Zhu,[b] N. Ghafoor,[b] M.P. Johansson,[b,c] J. Sjölen,[c] J. Jensen,[a] M. Odén,[b] L. Hultman,[a] and J. Rosén[a]

[a] Thin Film Physics Division, Department of Physics, Chemistry and Biology (IFM), Linköping University, SE-581 83 Linköping, Sweden
[b] Nanostructured Materials, Department of Physics, Chemistry and Biology (IFM), Linköping University, SE-581 83 Linköping, Sweden
[c] Seco Tools AB, SE 737 82 Fagersta, Sweden
*Corresponding author: ander@ifm.liu.se, phone +46 13 281251, fax +46 13 137568

Published in Surface & Coatings Technology 205 (2011) 3923-3930
DOI: 10.1016/j.surfcoat.2011.02.007

Abstract

This paper presents the physical mechanism behind the phenomenon of self-layering in thin films made by industrial scale cathodic arc deposition systems using compound Ti-Si-C cathodes and rotating substrate fixture. For the as-deposited films, electron microscopy and energy dispersive X-ray spectrometry reveals a trapezoid modulation in Si content in the substrate normal direction, with a period of 4 to 23 nm dependent on cathode configuration. This is caused by preferential resputtering of Si by the energetic deposition flux incident at high incidence angles, when the substrates are facing away from the cathodes. The Ti-rich sub-layers exhibit TiC grains with sizes up to 5 nm, while layers with high Si-content are less crystalline. The nanoindentation hardness of the films increases with decreasing layer thickness.

Keywords

Cathodic arc, Hard coatings, Layer formation, Ternary cathodes, Resputtering

1. Introduction

Cathodic arc is a powerful technique for thin film synthesis, where the plasma originates from so called cathode spots of very high current, power, and plasma density [1]. The resulting energetic and highly ionized plasma can be used for rapid growth of stable as well as metastable compounds, hence frequently used for tribological, decorative, protective, and functional coatings. Cathodic arc is in particular used extensively for commercial wear resistant coatings such as TiAlN [2], AlCrN [3], and TiSiN [4].

In a variety of applications, particularly at industrial scale, the aim is to coat large areas with high uniformity. As with other PVD-methods, arc deposition is a line of sight method, which necessitates rotation to equally expose all areas to the deposition flux when substrates are large or numerous. Substrate rotation, however, may induce an artificial layering of the coatings, see e.g. Ref. 5 and Ref. 6, due to anisotropic growth conditions. For many applications, this is used advantageously to create multilayers [7], where the large number of interfaces contributes to enhanced mechanical properties [8]. However, in most cases, the layering is unintentional and not even recognized. The underlying conditions during film growth, and the effects on the film properties have, so far, not been given much consideration. An improved understanding of these phenomena could have implications on the design of coatings as well as deposition systems. Sample fixture rotation and variation of coating flux by angular position have also been pointed out as an important underexplored factor for improved performance of coated products [9].

There are few studies focusing on properties of arc plasma originating from compound cathodes, despite their common use in a wide range of applications to enable synthesis of multi-element films through rational utilization of existing coating equipment. Here, we examine arcing from ternary Ti_3SiC_2 cathodes and the self-layering in the resulting Ti-Si-C coatings. The investigated cathodes are of relevance for exploration of, e.g., the Ti-Si-C-N system providing a path to coatings rich in both Si and C when used in reactive N_2 atmosphere [10]. We study the variation in film composition and structure with substrate position and cathode configuration, enabling analysis of the spatial deposition profile of each of the three elements. In conjunction with analysis of temporal changes in deposition conditions due to substrate rotation, we identify likely mechanisms for the layer formation. The findings emphasize the complex nature of material transfer from cathode to substrate

during cathodic arc deposition, particularly when employing compound cathodes combining lighter and heavier elements.

2. Experimental Details

Thin films were deposited using a Sulzer Metaplas MZR 323 industrial scale cathodic arc evaporation system, see schematic in Fig. 1. The chamber can hold up to six cathodes (diameter 63 mm) in simultaneous operation, placed on the left (L1-L3) and the right (R1-R3) side. The vertical cathode positions on opposite sides, i.e. L1 relative to R1 etc., are displaced about 10 cm relative to each other, to attain film thickness uniformity. Ternary Ti_3SiC_2 cathodes (Maxthal) were used in different configurations, and polished 12x12 mm cemented carbide substrates, WC with 10 wt% Co, were placed on a cylinder rotating at 3 rpm about 15 cm in front of the cathodes. During one revolution the substrates (S) experience passage in front of one cathode, L2, on one chamber side and in the space between two cathodes, R1 and R2, on the opposite side, see Fig. 1a. Further complex sample fixturing, such as three-fold rotation, is often used for specific applications. The present configuration was chosen to isolate one type of rotation and provide flexibility in substrate positioning.

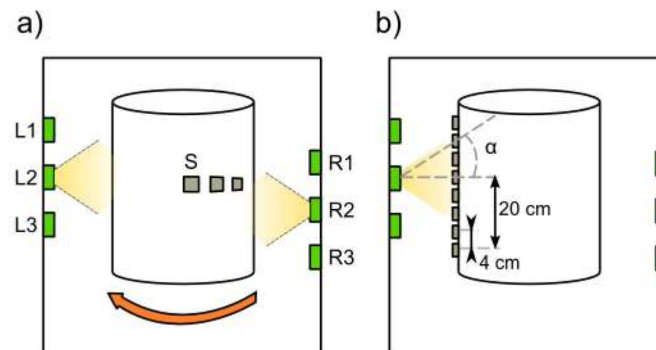

Figure 1 (a) Schematic drawing of the deposition chamber holding six cathodes, L1-L3 and R1-R3, and substrates S on a rotating metal cylinder. (b) A non-rotating chamber configuration for investigation of film thickness and compositional distribution.

The films were deposited using 50 A dc arc current at ~ $1x10^{-3}$ Pa base pressure. An addition of ~0.1 Pa Ar was necessary to sustain the arc. The substrates were negatively biased at -30 V, and the chamber was heated through resistive heating element located on the far chamber side, to approximately 400 °C on the rotating cylinder.

In the initial film growth five cathodes, L1-L3 and R1-R2, were operated, with substrates at position S, see Fig. 1a. In a second set of experiments, one cathode on

either left (L2) or right (R2) side, or on both sides (L2+R2) simultaneously, was used with substrates fixed at position S. In a final experiment, thicker films were deposited from one cathode (L2) without rotation of the cylinder. Substrates were then placed at approximately every 4 cm vertically covering a range of 20 cm below and above the cathode, see Fig. 1b. The latter stationary experiment was used for two purposes: i) to grow sufficiently thick films for compositional characterization, also on substrates placed far from the cathode within reasonable time, and ii) to isolate effects of relative cathode-substrate placement in the vertical direction only, as rotation would infer constantly changing horizontal positions.

Compositional characterization of the films, along with a cut-out piece from the cathode bulk, was carried out by elastic recoil detection analysis with a time-of-flight and energy detector (TOF-E ERDA), using a 40 MeV $^{127}I^{9+}$ ion beam at 67.5° incidence angle relative to the surface normal and 45° scattering angle. The resulting time-of-flight versus recoil energy spectra were evaluated using the CONTES code to obtain elemental composition spectra [11]. Structural characterization was performed trough transmission electron microscopy (TEM) and scanning transmission electron microscopy (STEM), using an analytical FEI Tecnai G2 TF 20 UT microscope equipped with an energy dispersive X-ray spectrometer (EDS). Cross sectional TEM samples were prepared through mechanical polishing and ion milling. X-ray diffractometry (XRD) for phase analysis was performed using a Bruker AXS D8-advanced X-ray diffractometer with a line-focus Cu K_{α} X-ray source. Film thickness was determined using a LEO 1550 Gemini scanning electron microscope (SEM), also equipped with Oxford Link EDS, on polished cross-sections. Film hardness was measurement on polished tapered cross sections using a UMIS nanoindenter equipped with a Berkovich diamond tip. Approximately 20 indents were made for each sample to an indentation depth of ~0.2 µm, corresponding to a maximum applied load of 25 mN. Hardness was evaluated using the method proposed by Oliver and Pharr [12].

3. Results and Discussion

Films deposited using the conventional five cathode setup features alternating bright and dark layers in a trapezoid wave pattern in bright field TEM, see Fig. 2a-b. The layering is even better revealed by z-contrast in STEM imaging, see Fig. 2c, together with EDS elemental mapping in a 50x50 nm^2 area, as shown in the inset. The amount of Si and Ti vary, with every second layer richer in Si (corresponding to bright region in the Si map) and with less of Ti. An EDS line profile (S→F), covering approximately

six periods, was recorded and is presented for Ti and Si in Fig. 2d as relative deviation from the respective average EDS signal. There is an anti-correlation between Si and Ti, with the Si oscillations being most pronounced, up to ± 20% of measured EDS signal. The profiles resemble a square wave with substantial noise. The segments where Si has positive deviation correspond to the dark regions in the STEM image, also indicated at the bottom of Fig. 2d (tolerating single deviating data points). The Si-rich regions are on average 12.4 nm thick, calculated over three 150 nm scans, compared to 10.9 nm regions where Ti has positive deviation. The Ti-rich zones also have larger crystalline grains as evident from dark field and high-resolution TEM, see Fig. 3a and b, respectively. In STEM the grains appear bright, see Fig. 2c, which together with the selected area electron diffraction (SAED) pattern inset in Fig. 3c indicate that these are TiC. Si has a known effect as grain refiner [4, 13] explaining the nanocrystalline grains in the Si-rich regions. The sub-layers within the Ti-rich regions, visible in Fig. 2 b and c, are related to passage between off-axis cathodes (R in Fig. 1a), and is discussed in detail below.

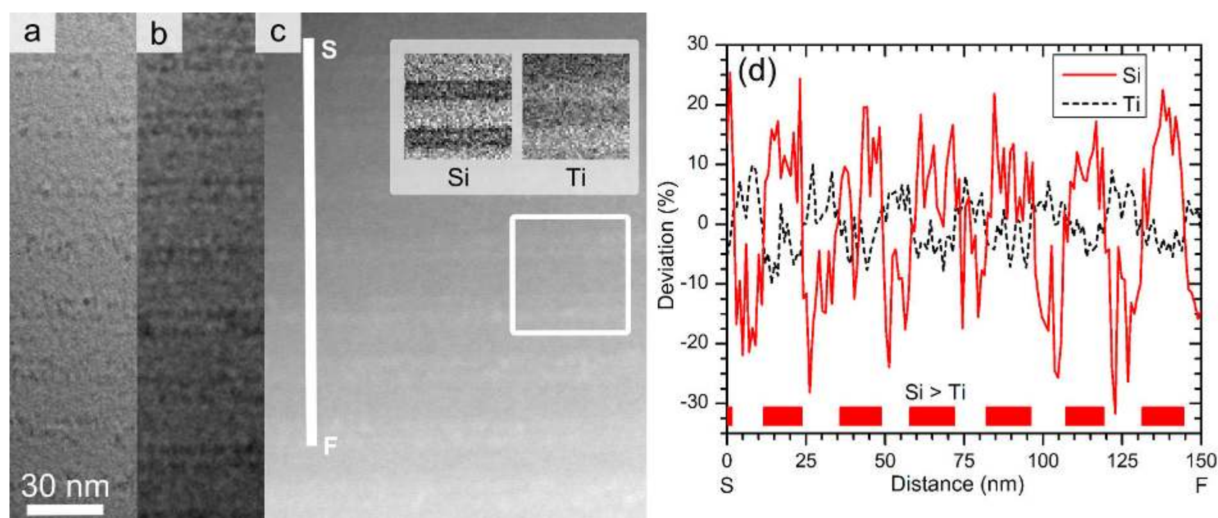

Figure 2 TEM micrograph displaying layering from the five-cathode setup acquired (a) in foucs, (b) at defocus which enhances contrast, and (c) in STEM mode with corresponding EDS-mapping. The EDS line profile from S to F indicated in (c) is presented in (d) for Ti and Si as deviation from average intensity. Regions where Si exceeds Ti, excluding single data points, are indicated at the bottom of (d).

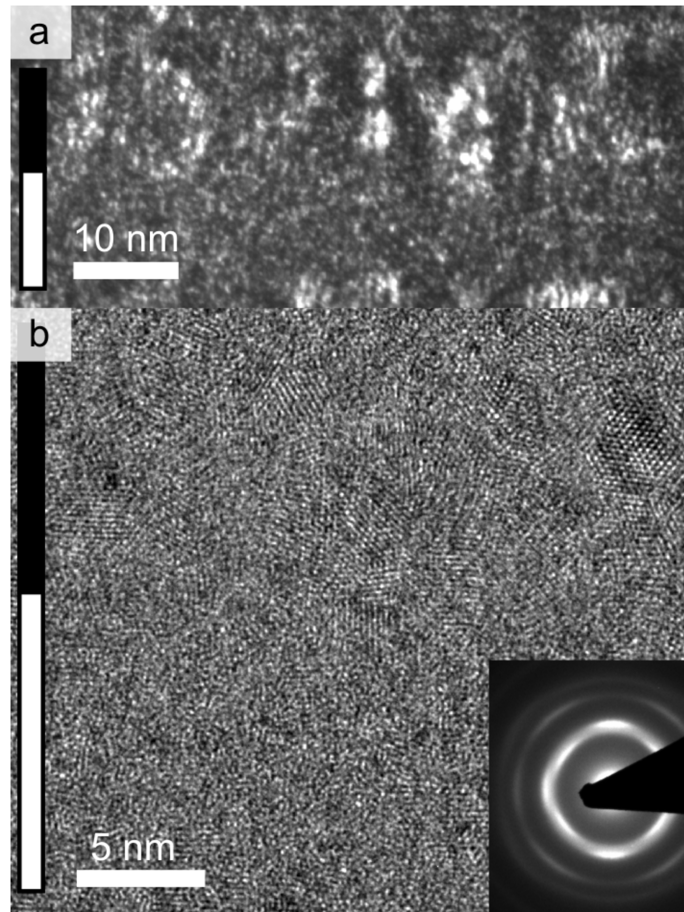

Figure 3 (a) Dark field, from the 200-reflection, and (b) high resolution TEM images of one layer period. The Ti and Si-rich regions are indicated with black and white markers, respectively.

The layered structure is present also in single cathode (L2) depositions, see Fig. 4a, when the substrate is placed on the rotating fixture directly in front of the cathode. STEM-imaging in Fig. 4b shows repeating broader bright and narrower dark segments, indicating compositional modulation similar to the five cathode case. Samples placed on the cylinder at 10 cm vertical displacement relative to the cathode center, under otherwise identical deposition conditions, have no discernible layering, see Fig. 4c. This result is confirmed by repeated analysis for a second off-axis sample from a different deposition under the same conditions. In the case where two cathodes were used (L2 and R2 in Fig. 1a), the layers are again present, see Fig. 4d, though with an increased thickness as compared to the one cathode case.

We conclude that layering with a characteristic appearance in terms of compositional modulation occurs in all cases when the substrate path includes passage directly in front of a cathode. The periodicity can be correlated to substrate rotation by knowing

the film thickness and deposition time, hence growth rate, together with rotation speed of the substrate holding cylinder. The growth during one full revolution corresponds to the size of the repeating motif.

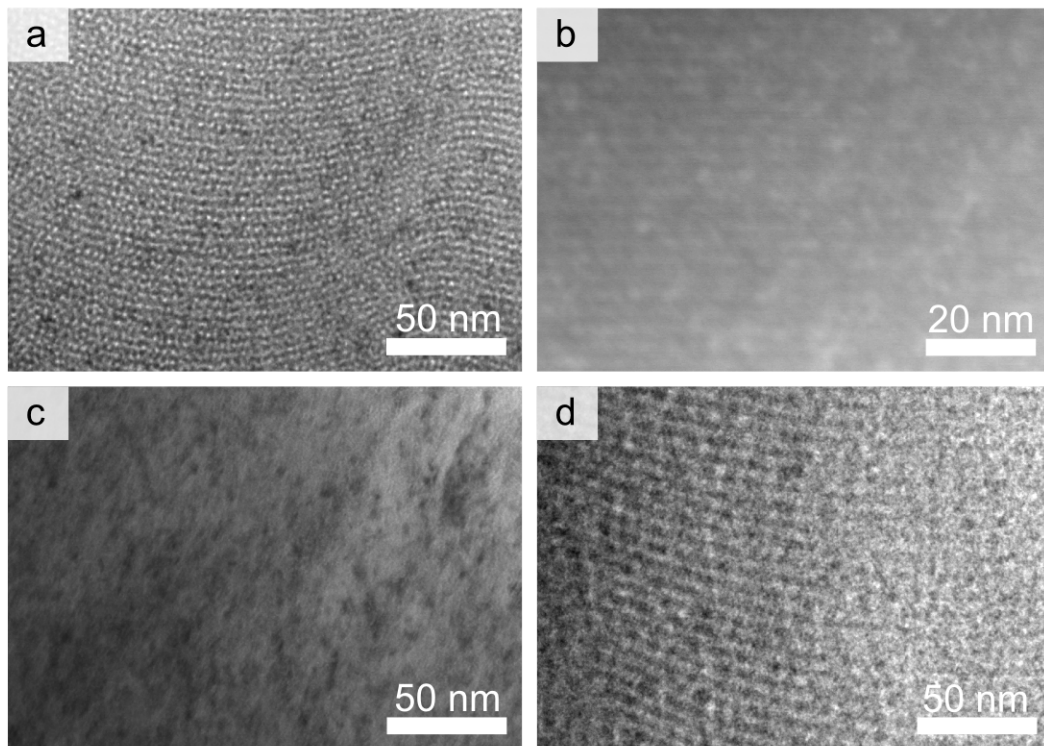

Figure 4 (a) TEM micrograph of film from single cathode (L2) deposition, with pronounced layer structure, and (b) corresponding STEM image indicating mass-contrast. (c) In the off-axis single cathode deposition no layers are visible. (d) An increased layer thickness, compared to (a), is evident for the two-cathode (L2 and R2) deposition.

All the investigated films are nanocrystalline with a grain or domain size generally below the thickness of the layer period. X-ray diffraction reveals only one identifiable film peak at a 2θ-angle of 41°, see Fig. 5. This is in the vicinity of the reference position for the Ti 101 reflection at 40.2° and the TiC 200 reflection at 41.7° [14]. Scans at 2θ-angles in the range 2-30° did not show any peaks originating from Ti_3SiC_2 MAX phase, which is the predominant phase in the cathode.

We suggest that the layering is primarily caused by selective re-sputtering in high plasma incidence angle segments of the rotation, after consideration of three potential factors: 1) spatial variations in plasma composition prior to deposition, 2) ion-surface interaction with resulting re-sputtering from the growing film, and 3) material transfer through post deposition processes, as outlined below. For

analysis of these factors, we initially assess the deposition profile from a single cathode onto stationary substrates, see Fig. 1b, thereby excluding effects from multiple cathodes as well as rotation.

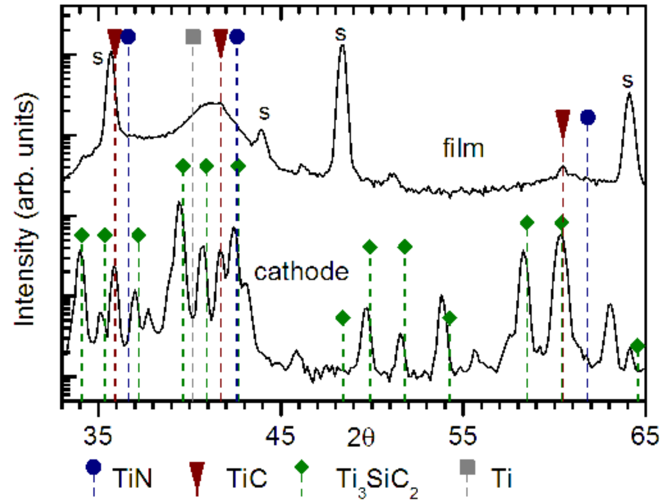

Figure 5 XRD diffractograms from virgin cathode and film deposited with five cathodes. Substrate peaks are denoted “s”.

The film composition profile from a non-rotating setup shows that the *relative* amount of Si peaks in front of the cathode, see Fig. 6a. A similar, but less pronounced, trend is indicated also for the Ti fraction. For off-axis positions, the composition changes towards less of Si (and Ti) and an increased fraction of C. The trends of Ti and Si were confirmed by corresponding EDS measurements (not presented here), excluding evaluation of C, N and O. Furthermore, oxygen contamination of 1-4 at% was present in all coatings, the levels correlated to pumping time prior to deposition. To interpret these results in terms of plasma distributions and absolute incorporation rate of the individual species, we need to consider the reduced flux off-axis from the cathode in addition to the relative composition given by ERDA. Hence, the film thickness was determined for the same samples that were compositionally profiled, see topmost curve in Fig. 6b. The thickness distribution is a measure of the *net* plasma flux onto the substrate, in other words, material that has been effectively deposited. The shape of the distribution is consistent with previous reports [15], with a strong angular dependence. The thickness is reduced to 10 % of the on-axis value at about 50° angle to the cathode surface normal.

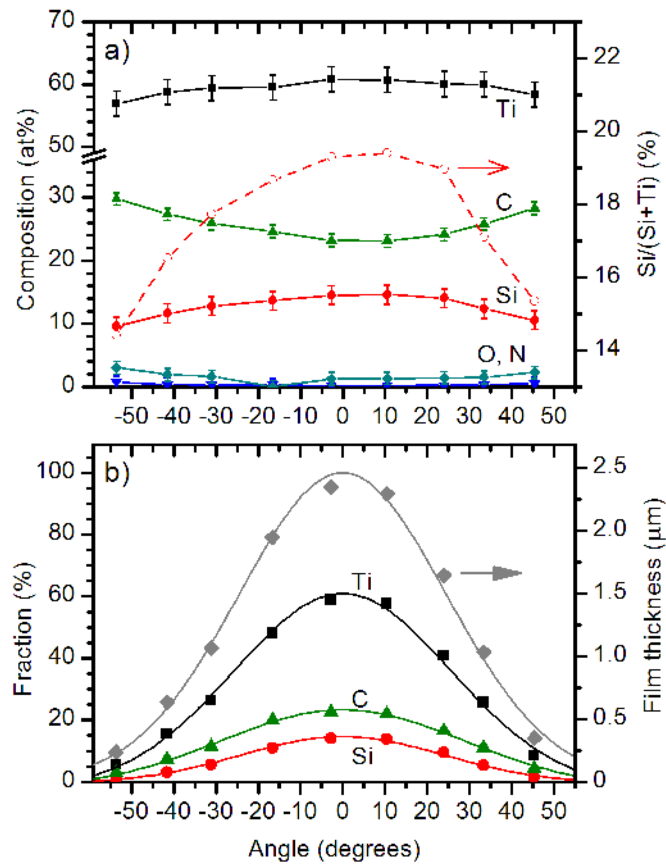

Figure 6 (a) Film composition obtained by ERDA, for samples at different vertical offset as shown in Fig. 1b. (b) Corresponding film thickness profile with Gaussian fit. The absolute elemental content is also indicated through multiplication of the film thickness distribution with the determined composition in (a).

The composition of Ti, Si, and C, given in Fig. 6b, is normalized with respect to maximum film thickness, and reflects the net plasma flux. The distributions are interpreted as absolute amounts of these elements, assuming that the compositional variation does not significantly affect film density. For all positions, the flux of Ti is largest, followed by C and Si, this order being in accordance with the cathode composition. The intensity profiles for Ti, Si, and C were fitted with Gaussian functions, see Fig. 6b, to model the experimental results. The determined functions were then used to project the distribution on a two-dimensional surface, with the angle to the cathode surface normal as parameter. The plots in Fig. 7 show the resulting distribution of net plasma flux of the different elements over vertical and horizontal angles. The path for a sample on the rotating cylinder at 13 cm vertical offset to the cathode center will be the approximated equivalent of following a trace in

Fig. 7 of constant vertical angle 40°. Strictly, the trace corresponds to movement on the plane parallel with the cathode and tangential to the cylinder, as probed in the vertical direction according to Fig. 1b. However, the approximation to the substrate path is reasonable since, within the angular range considered, the retraction relative to this plane caused by the cylinder curvature is relatively small, below 1 cm at 20° and ~4 cm at 40° horizontal angle. Therefore, one such cross-section (40° off axis) of the profile is given in Fig. 8a, together with the cross-section through the center of the profile, Fig. 8b. A quantitative comparison of the total plasma flux is obtained in these two cases by integrating the area under each curve. The distribution between the elements is similar, see inserted pie-charts, though with a noticeable decrease in Si for the off axis case.

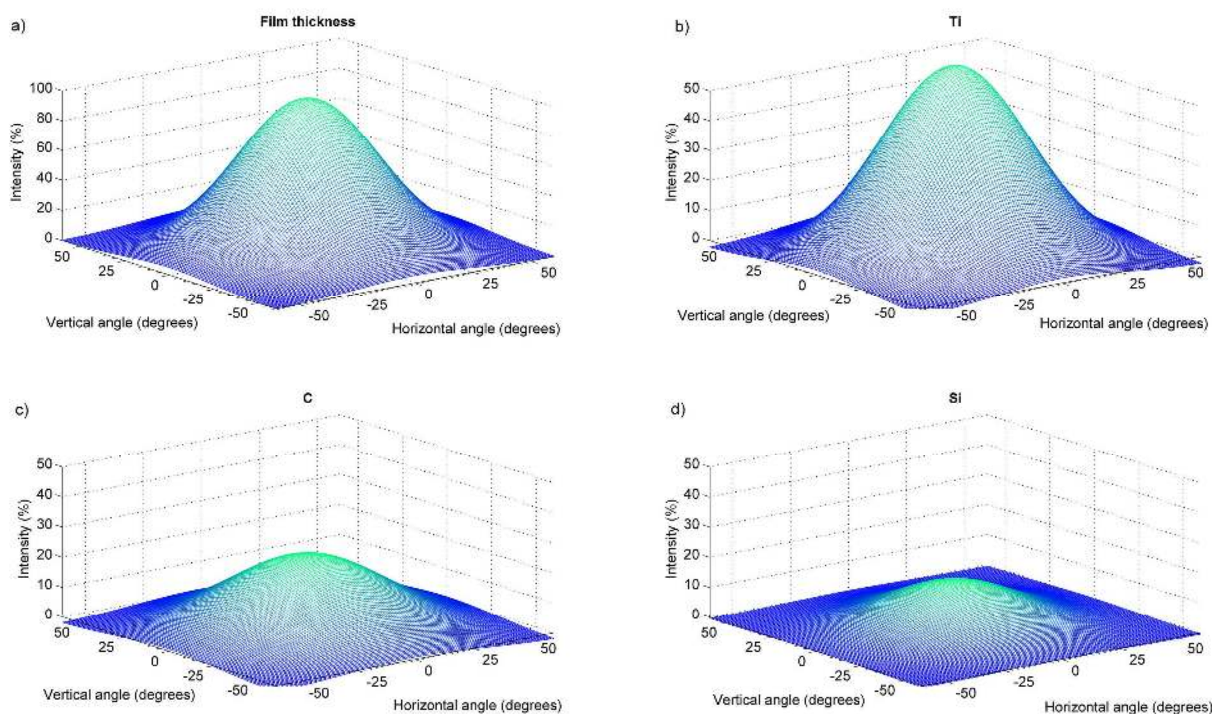

Figure 7 (a) Projected film thickness distribution over vertical and horizontal angles to the cathode surface normal, calculated by assuming rotational symmetry of the functions in Fig. 6b. Corresponding distributions of net plasma flux for (b) Ti, (c) Si, and (d) C, normalized to total peak flux, i.e. film thickness, at normal incidence in (a). Note the scale on the vertical axis in (a).

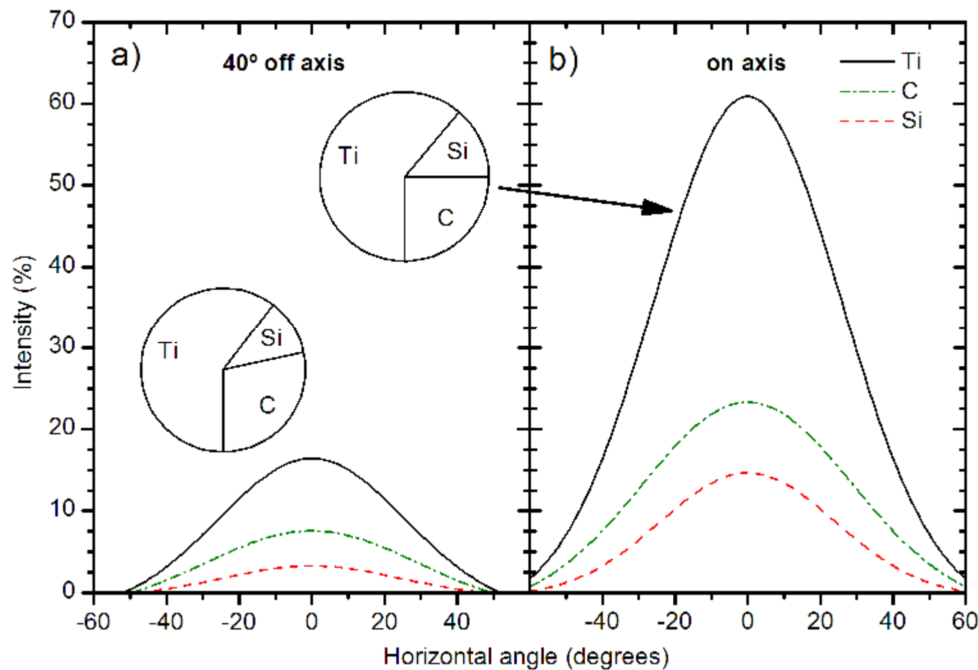

Figure 8 Comparison of relative net plasma flux intensity, from the distributions in Figure 7, for cross sections (a) off axis (40°) and (b) on axis. The pie-charts represent the integrated total flux for each cross section.

Layered films were here formed for deposition conditions with only one cathode active, as presented above, provided that the holding cylinder is rotated and the substrate passes in front of the cathode. Having established that film composition has an angular dependence, we henceforth discuss and evaluate plasma, surface, as well as film processes during deposition, to arrive at an explanation for this dependence as well as the observed layer formation.

3.1 Angular Dependence of the Plasma Composition

The arc plasma is considered to be generated from a point source, with a bell-shaped plasma density profile in the form of a Gaussian, cosine, or cosine^2 (etc.) distribution [15]. The details of the profile depend on plasma source design and geometry. The spatial distribution of evaporated material in pulsed arc has been studied by S. Anders *et al.* [16],, for different elemental cathodes. A tendency for broader distributions of elements with higher mass was found for metals in the range of 27 amu (Al) to 195 amu (Pt). A. Anders and G. Yushkov [17] found for C and Ti a good agreement with a cosine distribution within a 60° angle between the flux direction and the cathode surface normal. However, for larger angles, the detected flux was

more intense than predicted by the cosine distribution. Such compositional modulations of the plasma will likely result in compositional gradients in the films.

Our method to determine the angular variations of plasma composition is based on a combined analysis of film thickness and composition for substrates at various positions relative to one active cathode (L2 in Fig. 1a). Therefore, plasma conditions cannot be separated from processes affecting film composition during condensation and growth. Given this limitation, we observe an increase in the relative film composition of C (12.01 amu) and somewhat decreased levels of Si (28.09 amu) and Ti (47.87 amu) with increasing angle to the cathode normal, see Fig. 6a. This is apparently inconsistent with the reported elemental dependence of spatial plasma distribution at high angles discussed above [16, 17]. Scaling with film thickness does not reverse this trend as Ti is still more prominent in the peak-flux region than in the region at high angles, see Fig. 6b. Hence, our results on angular variation of film composition partly contradict anticipated trends based on results from single element cathodes. It also indicates that plasma flux variations alone are not sufficient to account for our observed compositional modulation in the films.

Along with plasma generation at the cathode surface, there is also formation of macroparticles. Since they spread preferentially at high angles [1, 18], the amount reaching the film may be somewhat higher at increasing angles from the cathode surface normal. If the macroparticles are assumed to have the cathode composition originating from the (presumed coherently) molten cathode material, these would be richer in Si and C than the overall coating. However, a resulting variation in film composition based on the macroparticle density is not consistent with measured spatial dependence of film composition. The macroparticles can thus not account for the observed layer formation.

3.2 Plasma Evolution During Transport

Cathodes of the nominal Ti_3SiC_2 stoichiometry were employed for this study. While the measured cathode composition corresponded to approximately 18 at.% Si, 30 at.% C, and 52 at.% Ti, the coatings contained substantially less Si, in most cases less C, and more Ti than the cathode, see Table 1. Incorporation of Ar was not detected in the films. Studies of the worn cathode surface indicate the presence of Si-rich phases $TiSi_2$ and $Ti_5Si_3(C)$ after evaporation [19]. Due to long deposition times in this study (usually 1-2 hours), steady state deposition is assumed where the total mass loss during plasma generation should be close to the cathode bulk composition.

Hence, at least part of the observed Si-deficiency in the films, which is dependent on substrate configuration, must be accounted for elsewhere. On the way from cathode to substrate the amount of Si could hypothetically be reduced due to: i) deflection, from elastic and inelastic collisions, or ii) plasma flux distributed at high angles and therefore not reaching the substrate. At 400 °C, Ar atoms have an average speed of ~600 m/s. At the present pressure (~0.1 Pa) this corresponds to a mean free path of ~18 cm. The arc plasma is expanding at a significantly higher speed, the most likely velocity reported for Ti is 15 400 m/s [20]. For Ti^{2+} ions moving in a background of assumed stationary Ar-atoms, the collision frequency will then be on the order of 1.3×10^{4} s^{-1}, applying kinetic theory [21]. The resulting mean free path of approximately 120 cm is well above the cathode to substrate distance ion our case. Collisions between expanding plasma ions and ambient gas atoms are hence infrequent. Furthermore, even when collisions take place, plasma-gas reactions are unlikely unless energetically favorable [22]. Finally, as mentioned above, the knowledge on the directional arc-plasma distribution [16, 17] does not indicate any preference for high-angle paths for Si.

Table 1 Film composition and hardness, for various cathode configurations.

Cylinder rotation speed	Cathodes used	Composition (at%) normalized to Ti + Si + C = 100 % Ti	Si	C	Hardness (GPa)
Non-rotating	L2	61.7	14.7	23.6	21.5 ± 0.5
3 rpm	L2	63.0	12.5	24.5	24.3 ± 0.6
3 rpm	L1-L3, R1-R2	60.7	10.5	28.9	22.0 ± 1.1
3 rpm	L2 & R2	60.9	10.5	28.6	24.6 ± 0.5
3 rpm	R2	61.1	9.8	29.1	25.9 ± 1.1
Nominal cathode composition		50.0	16.7	33.3	
Measured composition		52.2	17.6	30.2	

3.3 Ion Surface Interaction and Preferential Resputtering

To explain the Si-loss when comparing cathode versus film composition as well as layer formation during film growth, post-condensation processes, such as re-sputtering and re-evaporation, have to be considered. As a minor amount of Ar was present during synthesis, potential re-sputtering of Ti, Si, and C through

bombardment of Ti, Si, C or Ar is evaluated. Ti in arc plasmas is reported to have higher average kinetic energy (58,9 eV) compared to Si (34,5 eV) and C (18,7 eV) [1]. However, it should be noted that the ion energy distributions have an inherent high energy tail, up to hundreds of eV [23]. The average ion charge state in pulsed arc plasma follows the same trend, from Ti (2,03) and Si (1,39) to C (1,00) [1]. The kinetic energy gain across the potential difference between plasma and substrate (here biased to -30 V) is proportional to the individual charge state of the ion. The present study was conducted with dc-arc, but the ion charge states are assumed to follow a similar trend as previously reported [1]. Arc plasmas have been shown to exhibit significant self sputtering at substrate bias less than -50 V, as well as in absence of a bias [24]. Hence, this is also expected under the conditions used in our study. Furthermore, the formation of neutrals from initially fully ionized arc plasma interacting with surfaces, has most recently been demonstrated by Ni *et al.* through optical techniques [25]. This is further evidence of plasma-surface interactions creating secondary species under regular arc deposition conditions.

In the present study, Ti is the predominant projectile ion given its assumed higher kinetic energy, higher ion charge state, as well as higher relative abundance from the cathode composition of 50 at%. Even though most of the reference data for sputter yield involves noble gas ions in the range 0,1-100 keV, there is also a trend of highest yield for Ti followed by Si and C [26]. Furthermore, the sputter yield is strongly dependent on the incident angle of low-energy (~1 keV) projectile ions, increasing from normal incidence up to a maximum yield at 70-80° relative to substrate normal. The difference in sputter yield between normal and high incidence angle seems to be largest for lighter elements, with a more than twofold increase for the case of Ti and Al [27]. This is ascribed to increased occurrence of short anisotropic collision cascades near the surface. Recent results from arc depositions of various metals also indicate a lower effective sticking coefficient at higher ion incident angles, attributed to a combined effect of non-sticking and self-sputtering in the angular range 30° to 70° [28]. In our present configuration we can thus infer larger influence of sputtering for the segments of rotation leading up to and away from the position directly facing the cathode. The plasma incidence angle is changing rapidly due to the increasing horizontal distance to the cathode, a translation similar to moving to higher positions in Fig. 1b, with additional acceleration as the substrate normal is constantly perpendicular to the rotating cylinder surface successively facing away from, or towards, the cathode.

For the assessment of ion-surface interactions during growth, we conclude that the arc plasma processing infers self-sputtering on the substrates, with increasing efficiency at higher ion incidence angles. Ti, as the most abundant projectile ion, causes sputtering of primarily Si and C. Each full turn of the substrate holding cylinder has segments with low growth rate and high plasma incidence angle, where preferential re-sputtering can induce compositional changes in the near surface region, thereby inducing layer formation. In Fig. 9 we exemplify by following a substrate rotating in front of one active cathode, moving through the zones a-d for every revolution:

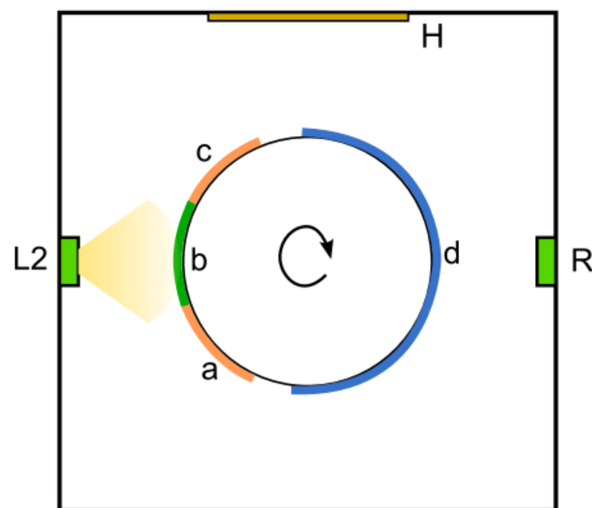

Figure 9 Schematic top view of chamber with one cathode (L2) running, while cathodes on the opposite side (R) are inactive, compare Fig. 1. Zone b, approximately -20° to 20°, is where majority of deposition occurs. In zones a & c the plasma flux is weaker, at large angle relative to the substrate normal, resulting in pronounced re-sputtering. In zone d the substrates are shielded from the plasma flux. The resistive heater H provides general heating for the chamber.

Zone b) The main part of the deposition occurs in zone b, with peak plasma flux close to normal incidence. Considering the angular dependence in Fig. 6b, 60 % of the film thickness obtained from one cathode passage will be deposited in the rotation segment with plasma incidence angles < 20°. In this region, high Si-content will promote a microstructure with small crystallites.

Zone a, c) In the sideways regions, a & c, the exposure is to less dense plasma where the fraction of Ti could be higher, interpreting Anders *et al.* [16]. As the ion incidence angle relative to the substrate normal increases, re-sputtering of primarily Si becomes more pronounced, coinciding with a decreased film

growth rate. This explains both the depletion of Si and C in the film as compared to the nominal cathode composition, and the stronger Si deficiency at increasing incidence angle of the plasma flux. The reduced Si content resulting from zone c allows formation of larger TiC grains, supposedly growing until the coating flux ceases, followed by re-initiation on the formed template when the substrate enters zone a.

Zone d) Outside the plasma flux region, in zone d, no deposition occurs, except for possible condensation of gaseous contaminants. The entire system is kept at a moderate temperature, hence providing limited energy for surface and bulk processes in the absence of plasma flux.

The above model of cyclic deposition and re-sputtering accounts for the layered structure after repeated exposure in zones a-d for every revolution. The thickness of the Si-depleted layers will be determined by the degree of re-sputtering, together with the effect of reduced growth rate in this region of high plasma incidence angles. This results in thinner Si-depleted layers, as compared to the Si-rich layers deposited with high growth rate for low angle plasma incidence. Similar layer formation has been briefly reported for other material systems and other cathode materials [5, 6], indicating that these types of effects occur relatively frequently when using rotating sample fixtures, though often disregarded or undetected.

3.4 Post-Deposition Processes

The film composition can be affected by secondary processes in the deposited film, and potentially cause Si-deficiency and contribute to layer formation. Substrates on the rotating cylinder are shielded from the plasma flux for a little more than half of each revolution, on the order of 10 s, that could be ample time for surface relaxation and diffusion. Hence, one possible mechanism for the loss of Si is through the formation of volatile Si species. Under the temperatures and pressures considered, only SiH_4 with critical temperature -3.5 °C [29] has a significant vapor pressure [30]. SiH_4 could be formed in reaction with hydrogen sources such as residual H_2O gas, though due to the low partial pressure of these gases they are not likely to contribute significantly to the formation of layers in our experiments.

Energy is required to overcome diffusion barriers and to initiate and sustain reactions. Apart from local heating by the plasma, the samples are subjected to the radiant heating to ~400 °C on the cylinder. As layer formation was not universal in thickness, and in some cases not even present, despite all samples being grown at the same

temperature, this energy contribution is likely too small to create Si-depleted zones up to 10 nm deep.

3.5 Multiple-cathode setups

When extending the configuration from one to two cathodes, the substrate will pass through the arc plasma flux twice every rotation. The repeating motif, however, corresponds also in this situation to growth during one revolution. No additional layers are formed as the cathodes are in different vertical positions, meaning that an on-axis trajectory with respect to substrate normal from the cathode center on the left hand side, in front of L2 in Fig. 1a, will be combined with a passage *off-axis* relative to R2. The plasma flux from R2, and resulting effects on the film, will therefore be similar to L2 passage in regions a and c in Fig. 9. Hence, no additional layer due to the second cathode is expected, only a slight increase in layer thickness. The flux from R2 will likely also cease more quickly when the sample rotates away from the cathode array.

The addition of more cathodes, up to the full capacity of six cathodes in this industrial deposition system, primarily enhances growth rate through overlapping plasma flux, particularly at off-axis positions. We note that the periodic intervals (the layer formation) are increasing from ~4 nm in the one cathode case up to ~23 nm for the five cathode configuration, but still corresponding to growth during one revolution. A narrow sub-layer within the Ti-rich region is indicated, see Fig. 2 a-b, which is likely an effect of local Si-enrichment caused by passage between cathodes R1 and R2, where their plasma intermix.

Comparing different cathode configurations, we note that the resulting film composition is similar in most cases, see Table 1, though with noticeable trends. There is a general increase in Ti, and a decrease in Si and C concentration, as compared to the nominal cathode composition. However, in the two cases where only one cathode (L2) is used, a relative increase in Si and decrease in C is observed compared to the other depositions. Furthermore, we note a higher Si content for the substrate in a fixed on-axis position compared to the rotating sample. The latter can be explained by re-sputtering, which is strongly dependent on cathode to substrate position, as discussed above. When the sample does not experience the high ion incidence angle segments following from rotation, the sputtering is not as pronounced. Preferential high-angle sputtering is likely also responsible for the compositional trends observed when adding more cathodes to the deposition

configuration. These cathodes provide additional plasma flux, though from a larger incidence angle towards the substrate.

3.6 Effect of Layers on Film Properties

The presence of layers, characterized by compositional gradients, is expected to influence the film properties. Table 1 presents the hardness of films deposited by five different cathode configurations. The hardness differences between the samples are comparatively small, yet significant with a measurement uncertainty corresponding to ± one standard deviation. There is a slightly varying composition of these films, as is also seen in Table 1, though not systematic with detected changes in hardness. However, two trends correlating hardness with layer formation are indicated: (1) Substrate rotation, and thereby formation of layers, increases hardness – compare cathode L2 with and without rotation. (2) An offset from the cathode reduces the layer period and induces an increased hardness – compare single cathode depositions for L2 and R2. Hardness of the films from the two-cathode deposition, L2 and R2, falls between these values, which is consistent with trend (2) suggested above.

4. Conclusions

We have studied the formation of compositionally modulated layers in Ti-Si-C thin films, formed during large-scale cathodic arc deposition onto substrates rotating in and out of the plasma flux. The layering can be attributed to resputtering of Si and C by Ti-ions during passages with high plasma incidence angle and low growth rate, in the segments of rotation leading up to and away from the cathode. The as-formed trapezoid wave modulated layer structures are characterized by sublayers with higher Si- and lower Ti-content, alternating with thinner sublayers of lower Si- and higher Ti-content. Crystallinity is also modulated, from ~5 nm TiC grains in the Ti-rich sublayers to nm-sized crystallites in Si-rich sublayers, due to the grain refining effect of Si. These artificial multilayer coatings have a slightly higher hardness compared to a coating deposited without rotation. When designing large scale arc deposition processes we advice attention to enhance benefits and mitigate drawbacks from the side effects of substrate rotation and self-sputtering inherent to cathodic arc.

Acknowledgment

This work was funded by the VINN Excellence center on Functional Nanoscale Materials (FunMat). The authors would also like to acknowledge Uppsala University for access to the Tandem Laboratory for ERDA-analysis.

References

[1] A. Anders, Cathodic Arcs, 1 ed., Springer, New York, 2008.

[2] S. PalDey, S.C. Deevi, Mat. Sci. Eng. A-Struct. 342 (2003) 58.

[3] J. Vetter, E. Lugscheider, S.S. Guerreiro, Surf. Coat. Technol. 98 (1998) 1233.

[4] A. Flink, M. Beckers, J. Sjölen, T. Larsson, S. Braun, L. Karlsson, L. Hultman, J. Mater. Res. 24 (2009) 2483

[5] J. Sjölén, L. Karlsson, S. Braun, R. Murdey, A. Hörling, L. Hultman, Surf. Coat. Technol. 201 (2007) 6392.

[6] A. Hörling, L. Hultman, M. Oden, J. Sjölen, L. Karlsson, J. Vac. Sci. Technol. A-Vac. Surf. Films 20 (2002) 1815.

[7] C. Ziebert, S. Ulrich, J. Vac. Sci. Technol. A 24 (2006) 554.

[8] H. Holleck, V. Schier, Surf. Coat. Technol. 76-77 (1995) 328.

[9] P.H. Mayrhofer, C. Mitterer, L. Hultman, H. Clemens, Prog. Mater. Sci. 51 (2006) 1032.

[10] A.O. Eriksson, J.Q. Zhu, N. Ghafoor, J. Jensen, G. Greczynski, M.P. Johansson, J. Sjölén, M. Odén, L. Hultman, J. Rosén, J. Mater. Res. (2011) DOI: 10.1557/jmr.2011.10

[11] M.S. Jansson, CONTES, Conversion of Time-Energy Spectra - a Program for ERDA Data Analysis, Uppsala University, 2004.

[12] W.C. Oliver, G.M. Pharr, J. Mater. Res. 7 (1992) 1564.

[13] L.J.S. Johnson, L. Rogström, M.P. Johansson, M. Odén, L. Hultman, Thin Solid Films 519 (2010) 1397.

[14] PDF: TiC 00-032-1383, Ti 00-044-1294, ICDD "Powder Diffraction File", 2008.

[15] I.G. Brown, Annu. Rev. Mater. Sci. 28 (1998) 243.

[16] S. Anders, S. Raoux, K. Krishnan, R.A. MacGill, I.G. Brown, J. Appl. Phys. 79 (1996) 6785.

[17] A. Anders, G.Y. Yushkov, Appl. Phys. Lett. 80 (2002) 2457

[18] J.E. Daalder, Journal of Physics D: Applied Physics 9 (1976) 2379.

[19] J.Q. Zhu, A.O. Eriksson, N. Ghafoor, M.P. Johansson, G. Greczynski, L. Hultman, J. Rosén, M. Odén, J.Vac.Sci.Technol. 9 (2011) 031601.

[20] A. Anders, G.Y. Yushkov, J. Appl. Phys. 91 (2002) 4824.

[21] P.W. Atkins, J. De Paula, Atkins' physical chemistry, Oxford Univ . Press, New York, 2002.

[22] E.W. McDaniel, Collision phenomena in ionized gases, Wiley, New York, 1964.

[23] J. Rosén, A. Anders, S. Mraz, J.M. Schneider, J. Appl. Phys. 97 (2005) 103306.

[24] A. Anders, Appl. Phys. Lett. 85 (2004) 6137.

[25] P.A. Ni, A. Anders, Journal of Physics D: Applied Physics 43 (2010) 135201.

[26] M.T. Robinson, Theoretical aspects of monocrystal sputtering, in: R. Behrisch (Ed.) Sputtering by particle bombardment. 1, Physical sputtering of single-element solids, Springer-Verlag, Berlin; New York, 1981.

[27] H. Oechsner, Applied Physics 8 (1975) 185.

[28] H.C. Wu, A. Anders, J. Phys. D-Appl. Phys. 43 (2010) 7.

[29] R.C. Weast, Handbook of chemistry and physics : a ready-reference book of chemical and physical data. Ed. 52, 52 ed., CRC, Cleveland, Ohio, 1971.

[30] D.R. Lide (Ed.) CRC Handbook of Chemistry and Physics, Ed 90, CRC Press, Boca Raton, Florida, 2009.